Electronic Supplementary Information:

Platinum-Nickel Nanowire Catalysts with Composition-Tunable Alloying and Faceting for Oxygen Reduction Reaction

Fangfang Chang[a, b], Gang Yu[a,*], Shiyao Shan[b], Zakiya Skeete[b], Jinfang Wu[b], Jin Luo[b], Yang Ren[c], Valeri Petkov[d,*], and Chuan-Jian Zhong[b,*]

[a] College of Chemistry and Chemical Engineering, Hunan University, Changsha 410082, China
[b]. Department of Chemistry, State University of New York at Binghamton, Binghamton, New York 13902, USA.
[c] X-ray Science Division, Advanced Photon Source, Argonne National Laboratory, Argonne, Illinois 60439, USA.
[d] Department of Physics, Central Michigan University, Mt. Pleasant, Michigan 48859, USA.

(* To whom correspondence should be addressed. Emails: cjzhong@binghamton.edu; yuganghnu@163.com; petko1vg@cmich.edu)

Additional Experimental Data:

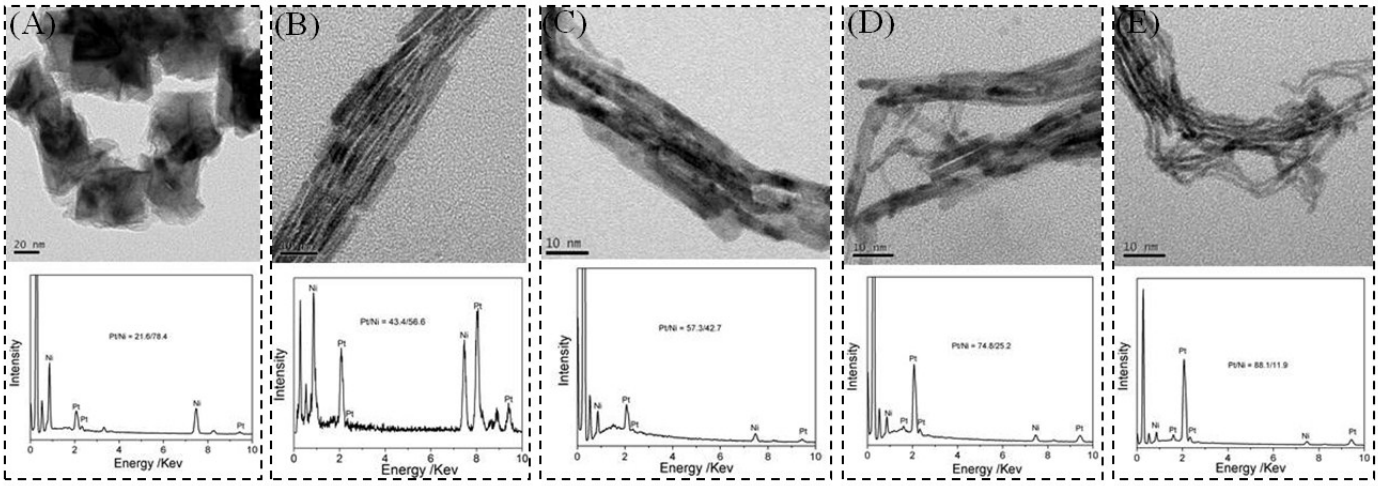

Figure S1. TEM images (upper) and EDX spectrum (lower panels) for $Pt_{22}Ni_{78}$ (A), $Pt_{42}Ni_{58}$ (B), $Pt_{57}Ni_{43}$ (C), $Pt_{75}Ni_{25}$ (D) and $Pt_{88}Ni_{12}$ (E)) NWs. The compositions are also confirmed by ICP-OES. The sizes are 20±2 nm, 3.3±0.5 nm, 2.0±0.5 nm, 3.0±0.6 nm and 3.0±0.5 nm. The standard deviation: 0.1%~0.5%.

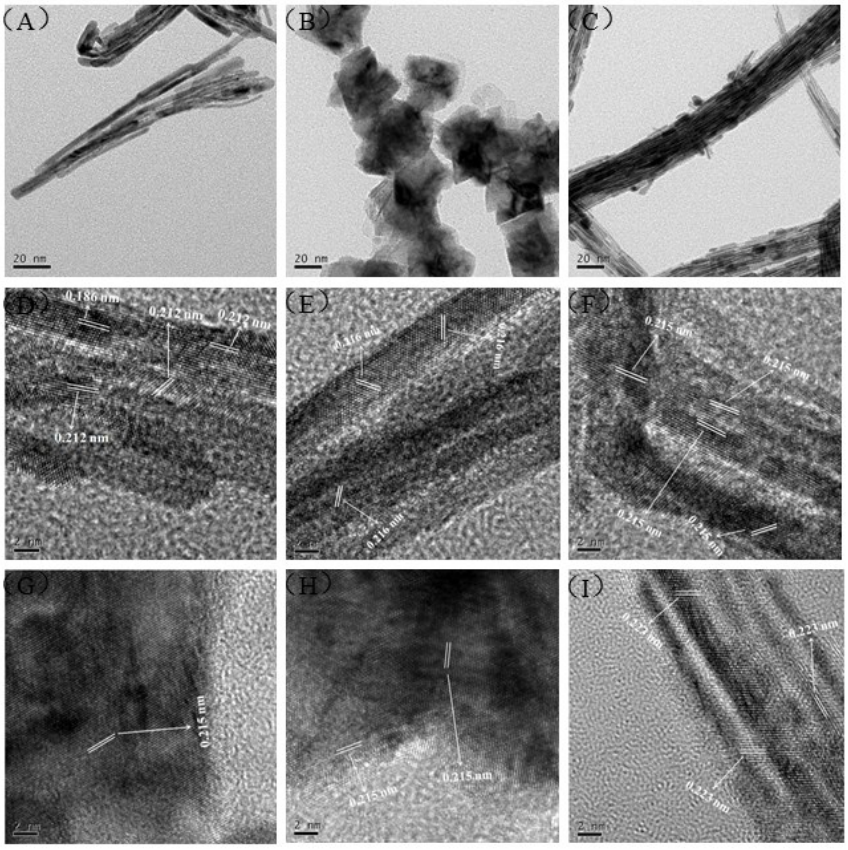

Figure S2. TEM images for $Pt_{57}Ni_{43}$ NWs (A), $Pt_{57}Ni_{43}$ NPs (B), and Pt NWs (C). The average feature sizes are 2.0±0.5 nm (diameter for individual boundled NW), 22±2 nm (diameter for individual cluster-like feature), and 2.0±0.2 nm (diameter for individual boundled NW) . HR-TEM images for as-synthesized $Pt_{57}Ni_{43}$ (D-F), D has (111) and (200) facets, E and F only have (111) facets, no (200) facets; as-synthesized $Pt_{57}Ni_{43}$ NPs (G-H), only have (111) facet, no (200) facets; as-synthesized Pt NWs (I), only have (111) facet, no (200) facets**.**

Table S1. Plot of percentages of relative facet domain sizes, $S_{(200)}$ vs. $S_{(111)}+S_{(200)}$ ($Pt_{22}Ni_{78}$; $Pt_{42}Ni_{58}$; $Pt_{57}Ni_{43}$ ($S_{(111)}/S_{(200)}$=5.5); $Pt_{75}Ni_{25}$ ($S_{(111)}/S_{(200)}$=4.0); and $Pt_{88}Ni_{12}$ ($S_{(111)}/S_{(200)}$=2.4)).

Catalysts	$Pt_{24}Ni_{76}$/C	$Pt_{43}Ni_{57}$/C	$Pt_{59}Ni_{41}$/C	$Pt_{78}Ni_{22}$/C	$Pt_{92}Ni_{8}$/C	Pt/C
Relative Ratio: (200)/[(200)+(111)]/%	0	0	15	20	23	0

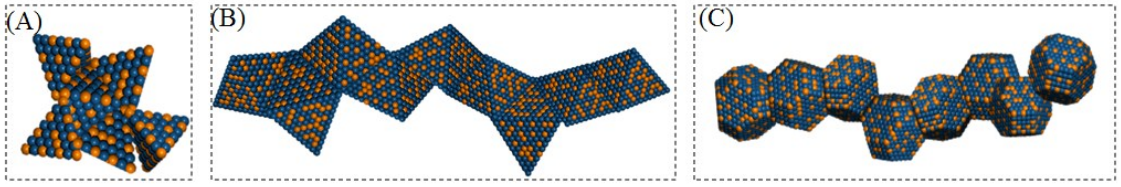

Scheme S1. Models for (A) a cluster of nano-tetrahedrons; (B) nanowire irregular Boerdijk–Coxeter helix of tetrahedrons with (111) facets; (C) nanowire of connected cubohedrons with both (111) and (200) facets.

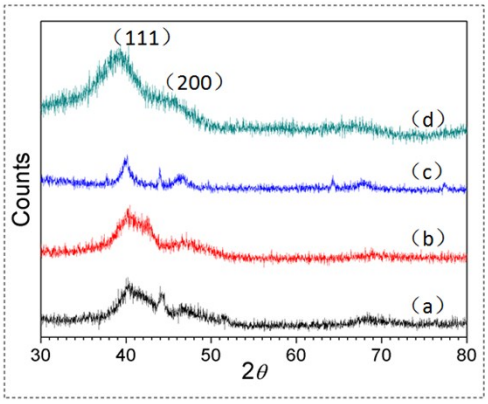

Figure S3. XRD patterns of NWs and NPs: (a) $Pt_{59}Ni_{41}$ NWs/C, (b) $Pt_{59}Ni_{41}$ NPs/C, (c) Pt NWs/C and (d) commercial Pt/C.

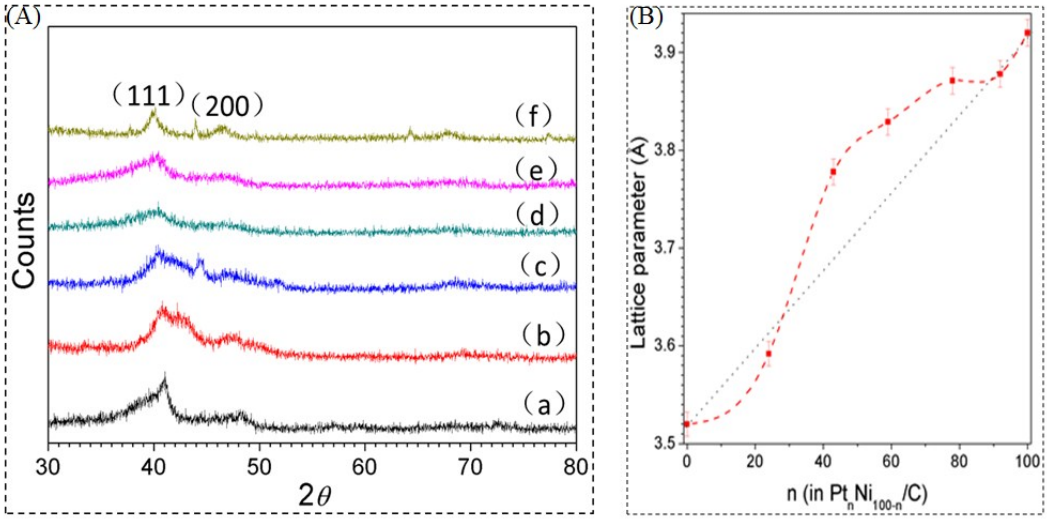

Figure S4. XRD patterns of NWs(A): (a) $Pt_{24}Ni_{76}$ NWs/C, (b) $Pt_{43}Ni_{57}$ NWs/C, (c) $Pt_{57}Ni_{43}$ NWs/C, (d) $Pt_{78}Ni_{22}$ NWs/C, (e) $Pt_{92}Ni_8$ NWs/C and (f) Pt NWs/C. (B) Dependence of the lattice parameters (symbols) for PtNi NWs/C on the relative composition of Pt%. The broken line is a linear fit to the experimental data.

Table S2**.** Current extraction in the kinetic region of PtNi NWs/C catalysts

sample	I_{limit} (mA) at 0.2V	I_{read} (mA) at 0.9V	I_K (mA) at 0.9V
$Pt_{24}Ni_{76}$/C	-0.6303	-0.1029	0.1230
$Pt_{43}Ni_{57}$/C	-1.0990	-0.2982	0.4092
$Pt_{59}Ni_{41}$/C	-1.1613	-0.3131	0.4286
$Pt_{78}Ni_{22}$/C	-1.1610	-0.3263	0.4540
$Pt_{92}Ni_8$/C	-1.1370	-0.2956	0.3994
Pt/C	-1.0485	-0.2115	0.2649

Table S3. Comparison of compositions, and ORR activities for different PtNi alloy catalysts

Catalyst	Mass activity (A/mg_{Pt}^{-1})	Specific activity(mA/cm^2)	Reference
$Pt_{56}Ni_{44}/C$	0.17	0.69	(S1)
Pt_3Ni/C	0.11	0.74	(S2)
PtNi/C	0.10	0.31	(S3)
Core–shell PtNi@Pt	0.03	0.13	(S4)
De-alloyed $PtNi_3$	0.29	1.49	(S5)
PtNi hollow nanoparticles	0.50	1.50	(S6)
PtNi octahedra	1.60	3.80	(S7)
PtNi nanoparticles	1.50	4.20	(S8)
Pt_3Ni NPs/MWNTs	0.85	2.67	(S9)
$Pt_{59}Ni_{41}/C$ NWs	0.33	0.61	This work

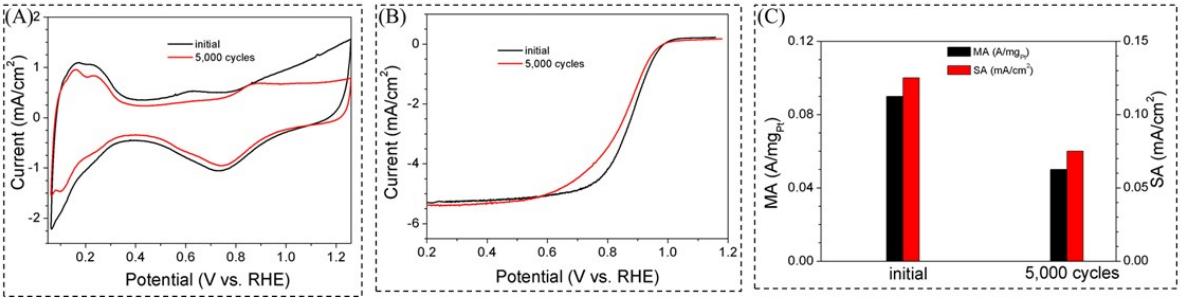

Figure S5. (A) CV and (B) RDE curves for commercial Pt/C before and after 5,000 potential cycles (sweep rate, 50mV/s, potential cycle window: 0.6 and 1.1 V) in 0.1 M $HClO_4$ solution saturated with nitrogen and oxygen (scan rate: 10 mV/s and rotation speed: 1600 rpm); (C) Mass activity and specific activity data at 0.900 V (vs. RHE) before and after 5,000 cycles.

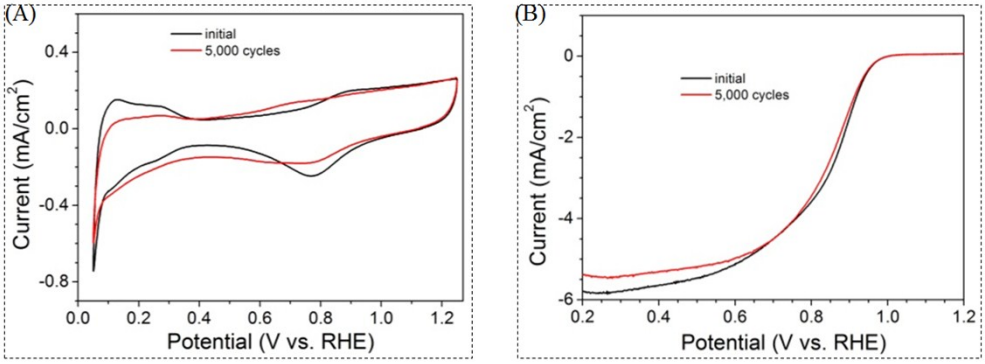

Figure S6. Durability test of $Pt_{59}Ni_{41}$ NWs/C catalyst for ORR. (A) CV curves at the beginning of potential cycling and at the end of 5,000 cycles (potential sweep rate, 50mV/s, potential cycle window: 0.6 and 1.1 V) in 0.1 M $HClO_4$ solution saturated with oxygen. (B) RDE curve for ORR at the beginning of potential cycling and at the end of 5,000 cycles (scan rate: 10 mV/s and rotation speed: 1600 rpm).

Electrocatalytic activity measurement

The electrochemically active area (ECA) of the catalyst was determined by the voltammetric charges for the adsorption of hydrogen on the Pt sites of the nanoalloy using the following equation.[S10]

$$\mathrm{ECA}\left[\mathrm{cm^2Pt/g\ of\ Pt}\right]=\frac{\mathrm{charge}\left[\mathrm{Q_H\mu C/cm^2}\right]}{210\left[\mathrm{\mu C/cm^2}\right]\times\mathrm{electrode\ loading}\left[\mathrm{g\ of\ Pt/cm^2}\right]} \qquad (1)$$

The diffusion limiting current is determined by the rate at which the reactant diffuses to the surface of the electrode. The current of the oxygen reduction reaction is dependent on the kinetic current (i_k) and diffusion limiting current (i_d):

$$\frac{1}{i}=\frac{1}{i_k}+\frac{1}{i_d} \quad (2)$$

The kinetic current is used to determine the mass activity (MA, current density per unit mass of Pt) and specific activity (SA, current density per unit area of Pt).

$$\mathrm{MA}=\frac{[\text{Kinetic current } i_k]}{[\text{catalyst amount on electrode}][\text{metal loading on carbon}][\text{Pt percentage}]} \quad (3)$$

$$\mathrm{SA}=\frac{\mathrm{MA}}{\mathrm{ECA}} \quad (4)$$

References

(S1) R. Loukrakpam, J. Luo, T. He, Y. S. Chen, Z. C. Xu, P. N. Njoki, B. N. Wanjala, B. Fang, D. Mott, J. Yin, J. Klar, B. Powell and C. J. Zhong, *J. Phys. Chem. C*, 2011, 115,1682–1694.

(S2) Z. W. Chen, D. Higgins, A. P. Yu, L. Zhang, J. J. Zhang, *Energy Environ. Sci.,* 2011, 4, 3167-3192.

(S3) W. K. Suha, P. Ganesana, B. Sonb, H. Kima, S. Shanmugam, *Int. J. Hydrogen Energy*, 2016, 41, 12983-12994.

(S4) W. Z. Li, P. Haldar, *Electrochem. Solid-State Lett*., 2010,13, 47–49.

(S5) F. Hasche, M. Oezaslan and P. Strasser, *J. Electrochem. Soc*., 2012, 159, 25–34.

(S6) S. J. Bae, S. J. Yoo, Y. Lim, S. Kim, Y. Lim, J. Choi, K. S. Nahm, S. J. Hwang, T. H. Lim, S. K. Kim and P. Kim, *J. Mater. Chem*., 2012, 22, 8820–8825.

(S7) C. Cui, L. Gan, M. Heggen, S. Rudi, P. Strasser, *Nature Materials*, 2013, 12, 765-771.

(S8) C. Wang, M. Chi, G. Wang, D. van der Vliet, D. Li, K. More, H. H. Wang, J. A. Schlueter, N. M. Markovic, V. R. Stamenkovic, *Adv. Funct.Mater.,* 2011, 21, 147-152.

(S9) J. Kim, S. W. Lee, C. Carlton, Y. Shao-Horn, *Electrochem. Solid-State. Lett*., 2011, 14, 110-113.

(S10) J. Luo, J. Yin, R. Loukrakpam, B. N. Wanjala, B. Fang, S. Shan, L. Yang, M. Nie, M. Ng, J. Kinzler, Y. S. Kim, K. K. Luo, C.J. Zhong, *J. Electroanal. Chem*, 2013, 688, 196-206.